A POWER-BALANCE MODEL OF L-MODE DENSITY LIMIT IN FUSION PLASMAS

P Zanca, F Sattin, Dominique F Escande

A POWER-BALANCE MODEL OF L-MODE DENSITY LIMIT IN FUSION PLASMAS

P. Zanca[1], F. Sattin[1], D. F. Escande[2], JET Contributors[3]

[1]Consorzio RFX (CNR, ENEA, INFN, Università di Padova, Acciaierie Venete Spa), Padova (Italy)

[2]Aix-Marseille Université, CNRS, PIIM, UMR 7345, Marseille, France

[3] see the author list of "X. Litaudon et al 2017 Nucl. Fusion 57 102001"

Abstract

A 1D cylindrical power-balance model of the radiation density limit gives a unified description of the phenomenon for stellarator, reversed field pinch and L-mode tokamak [P. Zanca et al, Nucl. Fusion **59** (2019) 126011]. The density limit scaling laws for the three different configurations are all derived by combination of just two equations: i) single-fluid heat-transport equation; ii) on-axis Ohm's law with Spitzer resistivity, taken in a suitable limit for the stellarator. Here, we present a refined version of the model, alongside further experimental evidences supporting its successful application.

1. Introduction

Density limit (DL) is ubiquitous in magnetic confinement fusion devices, and several processes can trigger this phenomenon. In particular, DL can take place as a radiation limit. In this regard, a 1D cylindrical power-balance model, matching fairly well experiments in the L-mode tokamak, in the reversed field pinch (RFP), and in the stellarator, derives a DL as bound of the equilibrium states characterized by realistic temperature profiles, i.e. with small values only at the edge, in the presence of radiation losses from impurities and edge neutrals [1, 2]. Differently from previous similar analyses [3-5], this model predicts the same DL expression for the tokamak and the RFP, without assumptions for the energy transport, but exploiting just two equations: i) single-fluid steady-state heat-transport equation; ii) on-axis Ohm's law with Spitzer resistivity. Within this model, the stellarator is approximated by a pure additionally heated cylindrical configuration. Since Ohm's law apparently does not apply to this case, the DL has been derived by the combination of i) with the International Stellarator Scaling 95 for the energy confinement time τ_E, as reported in [1, 2]. The expression obtained is very similar to the Sudo scaling [6], which represents the empirical reference for the stellarator, and it is also used for interpreting high-density experiments in Wendelstein 7-X [7]. However, in the present paper we will show that it is possible deriving an almost identical expression for the stellarator DL by combination of i) with a suitable limit of Ohm's law, thus removing any transport input, as done for the tokamak and the RFP. By limiting to just the couple of equations i),

ii) we obtain an even deeper unification of the DL modelling in the three major configurations. The generality of the model stems also from the fact that equation i) is implemented by taking radial integrals, a procedure that smooths out the profile peculiarities of the different configurations. Moreover, equation i) itself can be regarded as the cylindrical approximation of a flux-surface averaged equation. Given the minimal 1D physics involved, the model may represent the 'ultimate radiative DL'.

The paper is organized as follows. In section 2, a new and simpler method to integrate equation i) is presented. The basic DL relation is further developed by equation ii), providing the DL scaling laws for the different configurations. In section 3 a previous numerical analysis [1] of the same model is discussed. In section 4, the model is compared to specific experiments: some of them, already considered in [1, 2], are here revisited. Conclusions are drawn in section 5.

2. The model

In cylindrical geometry, we take the single-fluid steady-state heat transport equation

$$1)\quad \frac{d}{dr}\left(r\,K\,\frac{dT}{dr}\right) + r(\wp - \Re) = 0; \qquad \Re = n_e^2\,\mathcal{F}; \qquad \mathcal{F} = \left[\sum_j f_j Rad_j(T) + f_0 Rad_0(T)\right]$$

The single temperature approximation is justified by the strong coupling of ion and electron in the high density conditions we want to model ($T_i \approx T_e = T$). Here, K is an effective perpendicular conductivity, $\wp(r)$, $\Re(r)$ are respectively the heating power density (with ohmic and auxiliary components) and the radiated power density, n_e is the electron density. Moreover, f_j, Rad_j are the *j-th* impurity concentration and radiation rate coefficient respectively, whereas f_0, Rad_0 are the same quantities for neutrals. The main ion emission is discarded, as minor effect in the plasmas here considered. Throughout this paper we use the International System of units (SI), but for the temperature, which is expressed in keV. Therefore, K incorporates the numerical factor 1.6×10^{-16}. The temperature profile satisfies the on-axis symmetry condition $T'(0) = 0$ ($' = d/dr$). Moreover, the request of ambient temperature value at $r=a$, location of the first material wall, is modelled by the constraint $T(a)=0$.

Let's take the integral of (1) over $[0, a]$, after multiplying it by $rK\,dT/dr$:

$$2)\quad \frac{1}{2}\left[a\,K(a)\,\frac{dT}{dr}(a)\right]^2 = -\int_0^a r(\wp - \Re)\,r\,K\,\frac{dT}{dr}\,dr \geq 0$$

The inequality stems from the square in the l.h.s, and it will be transformed into a DL condition. We assume $\wp \ll \Re$ in the edge region, since both Rad_j, for light impurities, and f_0, for neutrals, are maximum there, due to the small temperature involved. We also assume that this is the *only* region where the above condition holds. The edge region is modelled by the radial and temperature intervals, $[r_*, a]$, $[0,\ T_* \equiv T(r_*)]$, with r_* close to a. Therefore, equation (2) can be approximated by

3) $\frac{1}{2}\left[a\,K(a)\,\frac{dT}{dr}(a)\right]^2 \approx -\int_0^{r_*} r\,(\wp - \Re) r K \frac{dT}{dr}\,dr + \int_{r_*}^{a} r^2 K\,\Re\,\frac{dT}{dr}\,dr \geq 0$

Now, we transform the two integrals of (3) separately. Taking into account the integral version of (1), $r\,K\,\frac{dT}{dr} = -\int_0^r \rho(\wp - \Re)d\rho$, the first integral over the plasma bulk $[0, r_*]$ (i.e. $[T_0 = T(0),\ T_*]$) becomes:

4) $\int_0^{r_*} r(\wp - \Re) r K \frac{dT}{dr}\,dr = -\frac{1}{2}\int_0^{r_*} \frac{d}{dr}\left[\int_0^r \rho(\wp - \Re)d\rho\right]^2 dr = -\frac{1}{2}\left[\int_0^{r_*} r\,\wp\,dr - \int_0^{r_*} r\,\Re\,dr\right]^2$

Since $\wp$ is small in the complementary narrow edge region, we approximate the integral $\int_0^{r_*} r\,\wp\,dr$ by the volume-average $\langle\wp\rangle$. Moreover, the integral $\int_0^{r_*} r\,\Re\,dr = \int_0^{r_*} r\,n_e^2\,\mathcal{F}\,dr$ is approximated by *representative average values* for density and $\mathcal{F}$ in the plasma bulk ($n_{bulk},\ \mathcal{F}_{bulk}$). Therefore

5) $\int_0^{r_*} r(\wp - \Re) r K \frac{dT}{dr}\,dr \approx -\frac{1}{2}\left[\frac{a^2}{2}\langle\wp\rangle - \frac{a^2}{2} n_{bulk}^2 \mathcal{F}_{bulk}\right]^2$;

$$\langle\wp\rangle = \frac{2}{a^2}\int_0^a r\,\wp\,dr\,; \qquad n_{bulk}^2 = \frac{2}{a^2}\int_0^{r_*} dr\,r\,n_e^2\,; \qquad \mathcal{F}_{bulk} = \int_{T_*}^{T_0} \mathcal{F}\,dT/(T_0 - T_*)$$

Now we address the edge integral of (3). Since r_* is close to a, we factor outside the integral the square of the radius, the conductivity and the density, by taking *representative edge values*, respectively a^2, $K(a)$, n_*:

6) $\int_{r_*}^{a} r^2 K\,\Re\,\frac{dT}{dr}\,dr \approx a^2\,K(a)\,n_*^2 \int_{r_*}^{a} \mathcal{F}\frac{dT}{dr}\,dr = -a^2\,K(a)\,n_*^2\,G_*; \qquad G_* = \int_0^{T_*} \mathcal{F}\,dT$

By replacing (5), (6) into (3) we obtain

7) $\frac{1}{2}\left[a\,K(a)\,\frac{dT}{dr}(a)\right]^2 \approx \frac{1}{2}\left[\frac{a^2}{2}\langle\wp\rangle - \frac{a^2}{2}n_{bulk}^2\mathcal{F}_{bulk}\right]^2 - a^2\,K(a)\,n_*^2\,G_* \geq 0$

This inequality provides the following DL condition

8) $[8\,G_*\,K(a)/a^2\,]^{\frac{1}{2}}\,n_* + n_{bulk}^2\mathcal{F}_{bulk} \leq \langle\wp\rangle$

The other possible solution, $\langle\wp\rangle \leq n_{bulk}^2\mathcal{F}_{bulk} - (8\,G_*\,K(a)/a^2\,)^{\frac{1}{2}}\,n_* < \langle\Re\rangle$, with $\langle\Re\rangle = 2\int_0^a r\,\Re\,dr/a^2$, is not physical for a steady state condition. Equation (8) is the same as equation (5) of [2], but here it has been derived by a simpler approach.

Now, we develop (8) by introducing the profile factor $\delta_n = n_{bulk}/n_*$, and the two densities

9) $n_1 = \langle\wp\rangle/[8\,G_*\,K(a)/a^2]^{\frac{1}{2}}$, $\qquad n_2 = (\langle\wp\rangle/\mathcal{F}_{bulk})^{1/2}$

with obvious meanings: n_1 is the DL for n_* neglecting bulk radiation ($\mathcal{F}_{bulk} = 0$; the approximation adopted in [1]); n_2 is the DL for n_{bulk} neglecting edge radiation ($G_* = 0$). After little algebra, the DL condition can be cast into the following equivalent forms, respectively for n_* and n_{bulk}:

10) $n_* \leq n_1 \times \Theta(\iota)$, $\quad n_{bulk} \leq n_1 \times \Theta(\iota) \times \delta_n$; $\qquad \Theta(\iota) = \left[(1+2\iota)^{\frac{1}{2}} - 1\right]/\iota$, $\quad \iota = 2\delta_n^2 n_1^2/n_2^2$

The function $\Theta \leq 1$ weighs the contributions of edge and bulk radiations. At the typical temperatures of the plasma bulk, the emission is important only for heavy impurities: by keeping them to negligible concentration, we have $n_2 \gg n_1$ and $\Theta{\sim}1$. In this case, n_1 is the fundamental quantity, whereas Θ can be regarded as a corrective factor.

The density n_1 contains an important dependence on $K(a)$, a quantity of not straightforward estimate. In the next paragraphs $K(a)$ will be replaced by global plasma parameters and a suitable profile

factor, by exploiting again equation (1) and the on-axis Ohm's law. This will provide the final DL scaling laws for the different configurations.

2.1 Tokamak and RFP expressions for n_1

Letting, $\kappa_a = 2 \times 10^{-6}\ K(a)/a^2$, $\hat{G}_* = 10^{35} \times G_*$, definition (9) for n_1 simplifies into

11) $n_1(10^{20} m^{-3}) = \frac{10^{1/2}}{2}\ \langle \wp(MW) \rangle\ /\ \left(\kappa_a\ \hat{G}_*\right)^{½}$

Both κ_a and $\hat{G}_*$ are $O(1)$ quantities: see following equations (20) and (28).

The factor κ_a can be replaced by T_0, by introducing an integral shape factor, which involves the normalized profiles $\hat{K} = K/K(a)$, $\hat{\wp} = \wp/\wp(0)$, $\hat{\Re} = \Re/\Re(r_*)$. To this purpose, we take a double integration of (1):

12) $\kappa_a\ T_0 = \langle \wp(MW) \rangle \times\ \Im_p;$ $\qquad\qquad \Im_p = \int_0^a dr\ \frac{1}{r\ \hat{K}} \left(\frac{\int_0^r dy\ y\ \hat{\wp}}{\int_0^a dy\ y\ \hat{\wp}} - \frac{\int_0^r dy\ y\ \hat{\Re}}{\int_0^a dy\ y\ \hat{\Re}} \right);$

When $\hat{\Re}$ is close to unity only at the edge, its contribution to $\Im_p$ is minor. In (12) we also exploit the condition $\langle \Re \rangle / \langle \wp \rangle = 1$, which holds at the DL, i.e. when equation (7) is satisfied as equality (see section 3).

Then T_0 is expressed by the on-axis ohm's law with Spitzer resistivity [4] (neoclassical effects vanish at $r = 0$). We take radially constant toroidal voltage $V_\phi = 2\pi\ R_0\ E_\phi$ (i.e. steady-state conditions; R_0 is the simulated major axis), by including the current drive effect (tokamak) and the RFP dynamo term:

13) $\hat{V}_\phi = V_\phi / [\xi(0)\ C(0)] = 2\pi\ R_0\ \eta(0)\ J_\phi(0) = 2\pi\ R_0\ \eta_1\ \zeta\ Z_{eff}\ T_0^{-\frac{3}{2}}\ J_\phi(0) \times 10^{-7},$

$$\eta_1 = 0.0165 \times ln\Lambda, \qquad \zeta = 0.58 + 0.74/\left(0.76 + Z_{eff}\right)$$

Z_{eff} is the plasma effective charge, and $ln\Lambda$ is the Coulomb logarithm: hereafter, we will fix $ln\Lambda = 15$, due to the weak dependence of the ensuing DL scaling laws on this quantity. The RFP anomaly function, $C(r) = E_\phi J_\phi / (\eta\ J^2)$, encapsulates the axisymmetric component of the non-linear perturbation term $\tilde{\mathbf{v}} \times \tilde{\mathbf{b}}$ in ohm's law (dynamo effect [8]). The current-drive function, $\xi(r) = J_\Omega / J$,

with J, J_Ω the current density magnitude, total and ohmic respectively, is related to the additional heating. We take $C = 1$ for the tokamak, and $\xi = 1$ in the absence of current drive. Note that the renormalized loop voltage $\hat{V}_\phi$ remains finite even in the presence of substantial current drive ($\xi \ll 1$, $V_\phi \ll 1$).

Finally, we replace the on-axis current density by the average current density, which is just the Greenwald parameter $n_G = I_P(MA)/(\pi a^2)$ [9]:

14) $J_\phi(0) = 10^6 \times J_\phi(0)/\langle J_\phi \rangle \times n_G$

This is convenient because the current profile factor $J_\phi(0)/\langle J_\phi \rangle$ partially offsets the previous one $\Im_p$. By combination of equations (11)-(14) we provide a family of four very similar n_1 scaling laws, given by the product of a purely ohmic Greenwald-like expression $n_{1,ohm}$, with an additional heating factor Π:

15) $n_1(10^{20}m^{-3}) = \Pi^{\frac{1}{2}} \times n_{1,ohm}, \quad n_{1,ohm} \cong 0.34 \times n_G^{\frac{5}{6}} \left(\zeta\, Z_{eff}\right)^{\frac{1}{3}} \hat{G}_*^{-\frac{1}{2}} \Psi_{G1} \left(\hat{V}_\phi/R_0\right)^{1/6}$,

16) $n_1(10^{20}m^{-3}) = \Pi^{\frac{1}{2}} \times n_{1,ohm}, \quad n_{1,ohm} = 0.25 \times n_G \left(\zeta\, Z_{eff}\right)^{1/2} \hat{G}_*^{-1/2} \Psi_{G2}\, T_0^{-1/4}$,

17) $n_1(10^{20}m^{-3}) = \Pi^{2/5} \times n_{1,ohm}, \quad n_{1,ohm} \cong 0.36 \times n_G^{\frac{4}{5}} \left(\zeta\, Z_{eff}\right)^{\frac{2}{5}} \hat{G}_*^{-\frac{1}{2}} \Psi_{G3}\, \kappa_a^{\frac{1}{10}}$,

18) $n_1(10^{20}m^{-3}) = \Pi^{4/9} \times n_{1,ohm}, \quad n_{1,ohm} \cong 0.23 \times n_G^{\frac{8}{9}} \left(\zeta\, Z_{eff}\right)^{\frac{4}{9}} \hat{G}_*^{-\frac{5}{9}} \Psi_{G4}\, (\Theta/\tau_E)^{\frac{1}{9}}$,

with

19) $\Pi = P/\left(\hat{V}_\phi I_p\right), \qquad P = \langle \wp \rangle \times 2\,\pi^2\, a^2 R_0$

Equation (18) is derived from (17) by replacing $\kappa_a^{1/10}$ with the energy confinement time:

20) $\kappa_a = 0.048 \times n_*(10^{20}m^{-3})/\tau_E\,\Psi_p, \qquad \Psi_p = \delta_{nT}\Im_p, \qquad \delta_{nT} = \langle n_e/n_* \times T/T_0\rangle$

This relation stems from the operative definition of τ_E in stationary conditions, $\tau_E = 1.6 \times 10^{-16} \times 3\langle n_e T\rangle/\langle \wp\rangle$, combined with (12). Equation (17) is approximately the scaling law considered in [1], (18) is exactly the scaling law obtained in [2], whereas (15), (16) are here presented for the first time. If the model was a perfect description of the reality, the above relations would be identical. Of course, this is not the case, and they can be taken separately, as different approximations of the DL. However, they compare almost in the same way to the experimental data.

For the additionally heated tokamak, Π is the power enhancement with respect to the ohmic heating. Obviously, $\Pi = 1$ for the ohmic tokamak. Though ohmic as well, Π is not exactly 1 for the RFP, due to the anomaly, defined below equation (13), which relates current and electric field:

21) $P = 4\pi^2 R_0 \int_0^a \eta\, J^2\, r dr = 4\pi^2 R_0 \int_0^a E_\phi\, J_\phi/C\, r\, dr = \hat{V}_\phi\, I_p \times \Pi; \quad \Pi = \int_0^a \frac{d}{dr}\left(\frac{rB_\theta}{a\,B_\theta(a)}\right)\hat{C}^{-1}\, dr$

Therefore, Π has the meaning of shape factor (close to unity) of the normalized anomaly profile $\hat{C} = C/C(0)$. The shape factors Ψ_{Gi} are similar combinations of those defined in (12) and (14):

22) $\Psi_{G1} = \left[J_\phi(0)/\langle J_\phi\rangle\right]^{1/3} \Im_p^{-1/2}, \; \Psi_{G2} = \left[J_\phi(0)/\langle J_\phi\rangle\right]^{1/6} \Psi_{G1} \quad , \quad \Psi_{G3} = {\Psi_{G1}}^{6/5} \quad , \quad \Psi_{G4} = {\Psi_{G1}}^{4/3}\, \Psi_p^{1/9}$

They can be estimated by computing normalized profiles for temperature and current with a scan of input profiles for thermal conductivity, additional heating and radiation, and then fitting the results by means of the measurable profile factors for temperature, $\delta_T = \langle T/T_0\rangle$, and density, δ_n (see appendix B of [2]). This analysis shows that $J_\phi(0)/\langle J_\phi\rangle$ and $\Im_p$ balance to some extent within Ψ_{Gi}.

Expressions (15)-(18) have been obtained without any modelling of transport: its effect has been encapsulated into global parameters by equations (12)-(14). In doing this, the linear P dependence of the initial equation (11) has been transformed into: i) a quasi-linear dependence on current, $n_{1,ohm} \sim n_G$, for an ohmic device; ii) a mixed power-current dependence, $n_1 \sim [P/\pi a^2]^{1/2}\ n_G^{1/2}$ for the additionally heated tokamak. The residual transport dependence of the final scaling laws is expressed by the weak confinement terms ${V_\phi}^{1/6}$, ${T_0}^{-1/4}$, ${\kappa_a}^{\frac{1}{10}}$, ${\tau_E}^{-1/9}$, by the integral of the normalized conductivity radial profile within Ψ_{Gi}, and by $\hat{V}_\phi$ within Π (anyway, $\hat{V}_\phi$ has limited variations with respect to those of P, I_p, in the tokamak).

Scaling laws (15)-(18) are *quantitatively* similar for the tokamak and the RFP: besides the comparable estimate of the shape terms Ψ_{Gi} (as expected, involving integrals of normalized profiles), the difference in the confinement order of magnitude of the two configurations is cancelled by the small exponents of the confinement terms: roughly speaking, passing from the tokamak to the RFP, V_ϕ, T_0, κ_a, τ_E vary by factors, $20, 10^{-1}, 10^2, 10^{-2}$ respectively, but ${V_\phi}^{1/6}$, ${T_0}^{-1/4}, {\kappa_a}^{1/10}, {\tau_E}^{-1/9}$ all vary only by a factor $1.6 \div 1.8$. Finally, we note that (15)-(18) do not depend neither on R_0, nor on the toroidal field B_ϕ.

2.2 n_1 for the stellarator

Semi-empirical, Sudo-like expressions for n_1 have been obtained for the stellarator, approximated by a pure additionally heated cylindrical configuration [1, 2]. In particular, the one reported in [2] stems from the initial DL relation (11), with κ_a replaced by τ_E (by means of (20)), and τ_E specified by the empirical International Stellarator scaling 95 [10], suitable to L-mode plasmas. It is

23) $\quad n_{1,ISS95}(10^{20} m^{-3}) \cong 0.257 \times P(MW)^{0.57}\ B_\phi^{0.33}\ R_0^{-0.54}\ a^{-0.72}\ \iota_{2/3}^{0.16}\ \left[\hat{G}_*\ \Psi_p\right]^{-0.4} [\delta_n/\Theta]^{0.2}$

with $\iota_{2/3}$ is the rotational transform at $r = 2/3\, a$.

Here, we obtain an almost identical expression by a suitable limit $V_\phi \to 0,\ I_p \to 0$ of the tokamak case discussed in the previous paragraph. This approach removes any empirical input. In the place of (14) we now use the standard relation

24) $J_\phi(0) = \frac{2}{\mu_0 R_0 q_0} B_\phi$

with q_0 the on-axis safety factor. Combination of (13), (24) gives

25) $0.25 \times \zeta \; Z_{eff} \; T_0^{-\frac{3}{2}} \; B_\phi \cong \hat{V}_\phi \; q_0 \equiv \lambda_{tok}$

Both q_0, $\hat{V}_\phi$ are close to unity for a tokamak, hence $\lambda_{tok}\sim 1$. Now, we decrease $\hat{V}_\phi, I_p$ towards zero at constant B_ϕ, at the same time increasing the additional heating to maintain T_0 constant. With the mild assumption that even Z_{eff} does not vary in this process, we can get arbitrarily close to a pure additionally heated cylindrical configuration, keeping (25) unaltered with the initial value $\lambda_{tok}\sim 1$. For such a configuration, a crude approximation of the stellarator, n_1 is then obtained by combination of (11), (12), (25):

26) $n_1(10^{20} m^{-3}) = 0.223 \times P(MW)^{1/2} \; B_\phi^{1/3} R_0^{-0.5} a^{-1} \left(\frac{\zeta Z_{eff}}{\lambda_{tok}}\right)^{1/3} \left[\hat{G}_* \; \Im_p \right]^{-1/2}$

The similarity of (23) and (26) is striking. Moreover, they are both very similar to the empirical Sudo-edge scaling $n_{Sudo\_edge}(10^{20} m^{-3}) = 0.2 \times P(MW)^{1/2} \; B_\phi^{1/2} R_0^{-0.5} a^{-1}$, proposed in [11] for the edge DL of LHD. Note that, (23), (26) depend on R_0, unlike (15)-(18).

2.3 The edge radiation term

The quantity $\hat{G}_*$, present in all the above DL scaling laws, can be given a simple approximate form [2]. First, denoting Z_i the main ion charge, we factor $Z_{eff} - Z_i$, taken radially constant, in the impurity term of $\mathcal{F}$ (see equation (1)):

27) $\hat{G}_* = 10^{35} \times \int_0^{T_*} \mathcal{F}\, dT = g_{I*} \times \left(Z_{eff} - Z_i\right) + 10^{35} \times f_0 \int_0^{T_*} Rad_0\, dT\,; \quad g_{I*}(T_*) = 10^{35} \times \int_0^{T_*} \frac{\sum_j \hat{f}_j Rad_j(T)}{\sum_j \hat{f}_j \left[Z_j^2(T) - Z_j(T) Z_i\right]}\, dT$

$Z_j(T)$ are the impurity charges, and $\hat{f}_j$ are the relative impurity concentrations (i.e. normalized to that of the dominant impurity). For light impurities, the integral function $g_{I*}(T_*)$ saturates quickly with T_*, approximately for $T_* \gtrsim 30eV$. The dependence of g_{I*} on the (light) impurity species is not strong, because $Rad_j(T)$ is divided by $Z_j^2(T) - Z_j(T)Z_i$ within the integrand, and the impurities with wider principal maximum in $Rad_j(T)$ also feature higher charge. For example, we estimate $g_{I*} \sim 4$ for Carbon and $g_{I*} \sim 4.8$ for Beryllium (we refer to the FLYCHK code [12, 13], for $Z_j(T)$), $Rad_j(T)$, as well as for $Rad_0(T)$). Therefore, in (27) the impurity species dependence is mainly transformed into the charge dependence $Z_{eff} - Z_i$. Second, we consider atomic line emission of Deuterium (D) to have a correct order of magnitude of Rad_0: taking $T_* \approx 50eV$, one gets $10^{35} \times \int_0^{T_*} Rad_0\, dT \approx 400 \approx 100 \times g_{I*}$. Therefore, (27) can be approximated by

28) $\hat{G}_* \approx g_{I*} \times \left[Z_{eff} - Z_i + f_0(\%)\right], \qquad g_{I*} \sim 4 \div 5$

Here, $f_0(\%)$ has the meaning of *effective concentration*, and weighs, by comparison with $Z_{eff} - Z_i$, the relative contributions of impurities and neutrals to the edge emission. Hereafter, approximation (28) will be adopted within all the scaling laws of the model.

3. Comparison with numerical analyses

A numerical analysis of the above set of equations, which improves some of the unavoidable approximations of the analytical approach (in particular $T(r)$ is computed from (1) self-consistently with $Rad_j(T)$), has been presented in [1] for the tokamak case. The DL is there identified by the boundary dividing the solutions with standard temperature profiles decreasing to small value at $r = a$, from the unphysical solutions featuring oscillating non-monotonic temperature profiles. The numerical DL agrees very well with the analytical DL, even though they somehow differ as far as the radiated power fraction, namely the ratio $\langle \mathfrak{R} \rangle / \langle \wp \rangle$, is concerned. In fact, the analytical DL, defined

by (7) taken as equality, corresponds to $T'(a) = 0$, which implies $\langle\Re\rangle/\langle\wp\rangle = 1$, as can be seen by the integral of (1) over $[0,\ a]$:

29) $\quad a\,K(a)\,\frac{dT}{dr}(a) = -\frac{a^2}{2}(\langle\wp\rangle - \langle\Re\rangle)$

Instead the numerical DL relaxes appreciably this condition, covering the interval $\langle\Re\rangle/\langle\wp\rangle \gtrsim 0.5$ (see figure 7 of [1]). This seeming contradiction is resolved by the non-linear relationship between $\langle\Re\rangle/\langle\wp\rangle$ and the proximity to the DL, namely the ratio $n_*/(n_*)_{DL}$. To illustrate this, let's assume that the radiation in the plasma bulk is negligible, namely $n_{bulk}^2\mathcal{F}_{bulk} \ll \langle\wp\rangle$ in equation (7). Therefore, $(n_*)_{DL} \cong n_1$, and by combination of (7), (9), (29) we get

30) $\quad n_*/n_1 \cong \sqrt{1-(1-\langle\Re\rangle/\langle\wp\rangle)^2}$

Owing to the non-linearity of (30), the narrow interval about the analytical DL $n_*/n_1 = 1$, covered by the numerical DL, corresponds to a significant range in $\langle\Re\rangle/\langle\wp\rangle$ (for example, taking $n_*/n_1 \gtrsim 0.9$ one gets $\langle\Re\rangle/\langle\wp\rangle \gtrsim 0.5$). In other words: the condition $n_*/n_1 = 1 = \langle\Re\rangle/\langle\wp\rangle$ of the analytical approach gives a good approximation of the more realistic numerical DL, which corresponds to an interval for $\langle\Re\rangle/\langle\wp\rangle$.

4. Comparison with experimental data

The model is now validated against data from several experiments, all obtained in conditions with negligible content of heavy impurities. Some of them have been already discussed in [1, 2], but they are presented again in a slightly refined form.

4.1 RFX-mod

The RFX-mod DL [14, 15] is taken as a term of comparison for the RFP. Since the line-average density $\bar{n}_e$ is the customary quantity stored in the RFX-mod databases, we estimate the correspondent DL, $(\bar{n}_e)_{DL} = n_1 \times \Theta \times \bar{\delta}$, by supplying the experimental peaking factor $\bar{\delta} = (\bar{n}_e/n_*)_{exp}$. In RFX-mod ($R_0 = 2,\ a = 0.46$), the density profile is rather flat, with a tendency to become hollow at high density: by taking $r_* = 0.9a$, inversion of interferometric data [16] provides the approximate trend

$\bar{\delta} \approx 0.73 \times \bar{n}_e(10^{20}m^{-3})^{-0.68}$. The ensuing DL scaling, $(\bar{n}_e)_{DL} \cong 0.83 \times (n_1 \times \Theta)^{0.6}$, features a very weak parametric dependence, when taking any of the expressions (15)-(18) for n_1. Therefore, we can safely replace all these parameters, but n_G, with typical, or at least reasonable values for RFX-mod. As an example, we specify n_1 by (18), and we set: $Z_i = 1$; $g_{I*} = 4$ (Carbon); $\tau_E = 10^{-3}s$; $\Theta = 1$ (given the flat/hollow density profile, we estimate $\Theta(2\,\delta_n^2\, n_{1,ohm}^2/n_2^2) \sim 1$; $\mathcal{F}_{bulk}$ within n_2 is computed for $T_0 = 0.2keV$, $T_* = 0.075keV$, according to the typical profile close to DL shown in figure C1 of [1]); with the definition (21) for Π, the global shape factor is estimated as $\Pi^{\frac{4}{9}}\,\Psi_{G4} \sim 3.8$ (see appendix B of [2] and appendix C of [1]). We approximately get a square root dependence on n_G:

31) $$(\bar{n}_e)_{DL}(10^{20}m^{-3}) \approx 0.764 \times \left(\zeta\, Z_{eff}\right)^{0.26} \left[f_0(\%) + Z_{eff} - 1\right]^{-0.33}\; n_G^{0.53}$$

The trend $Z_{eff} = 1 + 0.5/\bar{n}_e(10^{20}m^{-3})$ is a reasonable assumption for RFX-mod [17], considering also the weak dependence of (31) on this parameter. Figure 1 shows that (31) delimits fairly well the upper boundary of the RFX-mod operative $(n_G, \bar{n}_e)$ space (the database is the union of the two ensembles used for figures 1 of [14] and [15]). Instead, the $\bar{n}_e(10^{20}m^{-3}) = n_G$ criterion leaves a significant gap for $n_G > 1$. Note also that the experimental points tend to become sparse when approaching the boundary (31). In agreement with the general premise of the introduction, this suggests the interpretation of (31) as 'ultimate DL' (replacing the 'standard' n_G reference), but in the presence of other mechanisms, which hinder or prevent the density increase towards that limit. In fact, saturation of the density build-up due to high edge transport [18], and radiative instabilities related to the 3D magnetic topology [15], play a significant role.

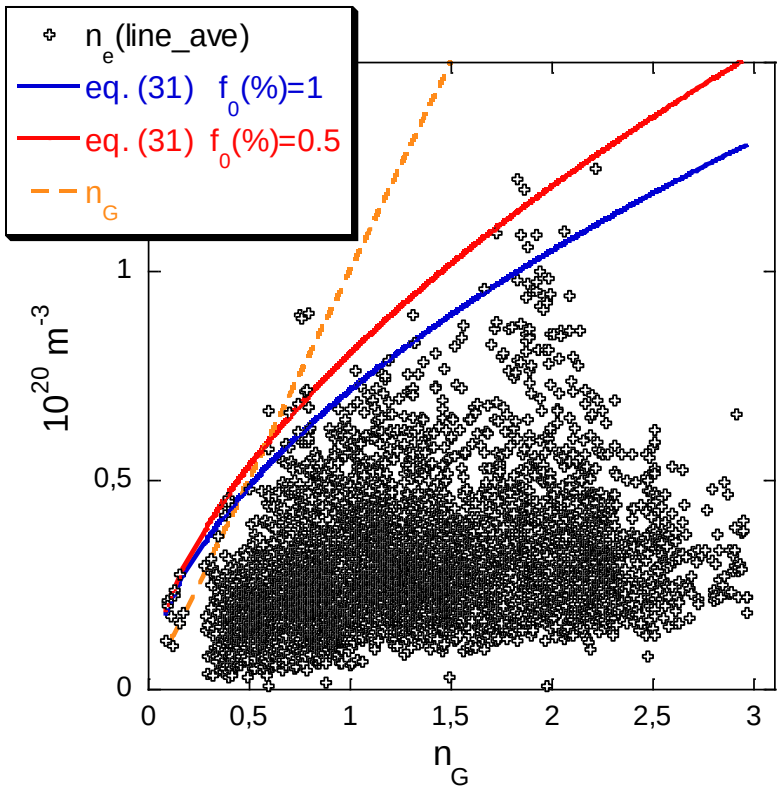

Figure 1. RFX-mod operative (n_G, $\bar{n}_e$) space. Predicted DL (31) is given for two values of f_0. The dashed line corresponds to $\bar{n}_e = n_G$.

4.2 FTU

The FTU ($R_0 = 0.935,\ a = 0.28$) ohmic tokamak experiments [19] are particularly relevant, because the edge DL ($r_*/a \sim 0.8$), which is straightforwardly compared to our model, is characterized there. The experimental densities reported in figure 11 of [19] are now compared to the prediction of the model, $(n_*)_{DL} = n_{1,ohm} \times \Theta$, taking (16) for $n_{1,ohm}$. We set $g_{I*} \approx 4.7$, assuming Boron as the dominant impurity (clean machine conditions are obtained by boronization), and $T_0 \approx 1$ (see figure 2 of [19]). The shape factor Ψ_{G2} is replaced by the average value ($\sim$2.68) estimated on the JET database discussed in the next paragraph, where we have access to profile information: this value is assumed to be representative of the L-mode tokamak. One gets

32) $(n_*)_{DL}(10^{20}m^{-3}) \approx 0.3 \times \left(\zeta\, Z_{eff}\right)^{1/2} \left[f_0(\%) + Z_{eff} - Z_i\right]^{-1/2} n_G \times \Theta$

The compatibility between (32) and the empirical scaling $(n_*)_{DL,exp}(10^{20}m^{-3}) \approx 0.34 \times n_G$ proposed in [19] is self-evident. Therefore, we compute (32) with $Z_i = 1$, $Z_{eff} = 1.25$ (it is reported $Z_{eff} < 1.5$), $f_0(\%) = 0.5$ (a value suggested by the above mentioned JET analysis), and with $\Theta(2\,\delta_n^2\, n_{1,ohm}^2/n_2^2)$ properly taken into account, since these discharges are characterized by a large variation of δ_n ($\mathcal{F}_{bulk}$ within n_2 is computed for $T_0 = 1$, $T_* = 0.075$). One gets $(n_*)_{DL}/(n_*)_{DL,exp} = 1.05 \pm 0.28$ (average and standard deviation). Same result with the empirical scaling: $0.34\, n_G/(n_*)_{DL,exp} = 1.06 \pm 0.28$

4.3 L-mode additionally heated JET experiments

The model prediction $(n_{bulk})_{DL} = n_1 \times \Theta \times \delta_n$, with (18) for n_1, has been compared in [2] to a set of about 40 high density disrupted, L-mode, JET discharges in divertor configuration ($R_0 = 2.98$, $a = 0.95$), both with Carbon wall (CW), and ITER-like wall (ILW: Beryllium for the first-wall, Tungsten for the divertor). Most of the shots feature NBI heating (up to 11MW), seven are purely ohmic, whereas ICRH ($\sim 4 \div 6\ MW$) is present only in a couple of shots, in combination with the NBI. The experimental signals for many of the needed quantities (in particular Z_{eff} and V_ϕ) are available. Apart one shot, which required the inclusion of a small amount of Tungsten, it was sufficient to restrict to light impurities and neutral Deuterium to make the model compatible with the maximum experimental volume-average densities $\langle n_e \rangle_{DL,exp}$. A slightly better agreement was also obtained by replacing some uncertain terms, such as the profile factors and the renormalized voltage $\hat{V}_\phi = V_\phi/\xi(0)$, with typical estimated values, possibly removing some noise in the prediction, thus highlighting the most important dependences. This *model reduction* is presented again, going deeper in the comparison with the database. Starting from $(n_{bulk})_{DL} = n_1 \times \Theta \times \delta_n$, with n_1 given by (18), we replace the product $\hat{V}_\phi^{\,-4/9}\, \Psi_{G4}\ \Theta^{10/9}\, \delta_n$ by its average value over the whole database (since the density profiles are weakly peaked, it is not crucial to take into account the exact shot by shot variation of δ_n), taking only the last $200ms$ before the disruption. We get:

33) $$(n_{bulk})_{DL}(10^{20}m^{-3}) \approx \mathrm{C} \times \frac{(\zeta\, Z_{eff})^{\frac{4}{9}}}{[f_0(\%)+Z_{eff}-Z_i]^{\frac{5}{9}}} \left[\frac{P(MW)}{\pi a^2}\right]^{4/9} n_G^{4/9}\ \tau_E^{-\frac{1}{9}}; \qquad \mathrm{C} = \frac{1.07 \pm 0.32}{g_*^{5/9}}$$

A tolerance deriving from the standard deviations of the above product is reported in C. Since $g_*\sim 4$ for Carbon and $g_*\sim 4.8$ for Beryllium, we expect $\mathsf{C}\sim 0.45 \pm 0.15$. Note that, both P and I_p are divided by πa^2 in (33). Expression (33) with $\mathsf{C}\approx 0.4$, $f_0(\%) = 0.5$ (a choice compatible with the typical relative contributions of impurity and neutrals to the edge radiation [20]) and approximation $\tau_E^{-1/9} \approx 1$ (suitable for JET), was the reduced scaling considered in [2]. Here instead, C and $f_0(\%)$ are optimized by a fit (in doing this we exclude the above mentioned peculiar shot). After dividing the experimental $\langle n_e \rangle_{DL,exp}$ by $[P(MW)/(\pi a^2)]^{4/9}\, n_G^{4/9}$, we take a two-parameters fit with the function $m_1 \times Z_{eff}^{\frac{4}{9}} \left[m_2 + Z_{eff} - Z_i\right]^{-\frac{5}{9}}$, representing the Z_{eff} dependence in (33) (all values are time-averaged over the last $200ms$ before the disruption; the weak factor ζ is discarded here, since its inclusion does not modify the result). The data, displayed in figure 2a), follows a weak decreasing trend with Z_{eff}, compatible with the model's prediction (a power law fit would be slightly worse). Since the optimum values, $m_1 = \mathsf{C} \times \tau_E^{-\frac{1}{9}} \sim 0.37$, $m_2 = f_0(\%) \sim 0.46$, are in the expected range for these parameters, the fit gives a confirmation of the model. The JET DL increased of about 20% when CW was replaced by ILW [21]: from figure 2a) this may be interpreted as an effect of the smaller Z_{eff}, which according to (28) implies lower edge radiation, passing from Carbon to Beryllium as dominant impurity. The model (33), with the fitted values for $\mathsf{C} \times \tau_E^{-\frac{1}{9}}$, $f_0(\%)$ is compared to the experimental DL in figure 2b). The vertical bars give the sensitivity from $f_0(\%)$ (upper and lower extremes correspond to 0.2 and 1 respectively): this is relevant for ILW discharges, due to their small $Z_{eff} - Z_i$. In any case, it is clear that the model aligns the disruptions, whereas the Greenwald parameter absolutely does not.

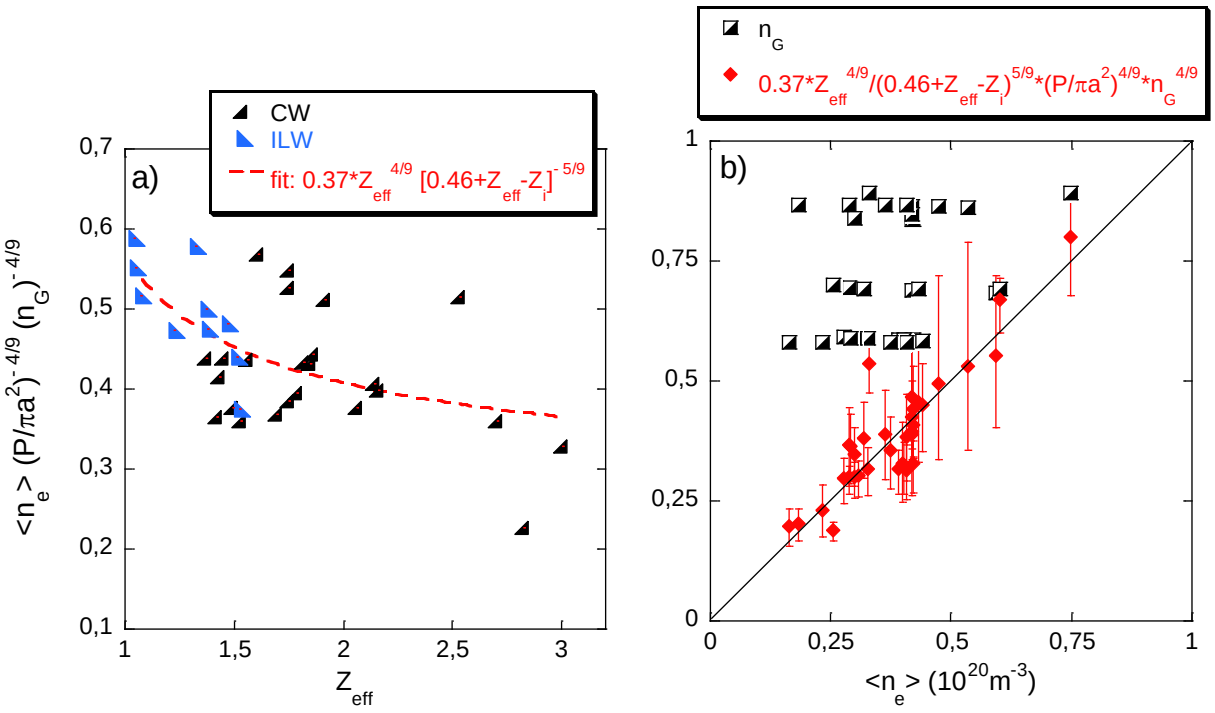

Figure 2. Data taken close to the disruptions. a) $\langle n_e(10^{20}m^{-3})\rangle[P(MW)/(\pi a^2)]^{-4/9}\, n_G^{-4/9}$ against Z_{eff}: ILW (blue triangles), CW (black triangles), fit (red line). b) scaling (33) (red diamond) and n_G (squares) against experimental $\langle n_e\rangle_{DL,exp}$; vertical bars gives the interval of model prediction for $f_0(\%) = 0.2 \div 1$.

The DL of our model does not depend on the additional heating system: any difference in the power deposition profile from one heating method to another is smoothed out by the double radial integration of the shape term $\Im_p$ in equation (12). In the above database, no appreciable dependence of DL on the heating technique is found (see figure 9 of [2]), but too few shots with ICRH are there to draw a sound conclusion.

After publication of [2], we considered previous L-mode JET experiments in limiter configuration, which demonstrate the complete equivalence of ICRH and NBI as far as DL is concerned [22, 23]. This result is achieved by some optimizations which minimize the impurity production specific to ICRH. In figure 3 model (33) is compared to three examples of these experiments, taken from figure 2 of [22], all with $I_p = 3MA$ and similar Z_{eff} (see figure 4 of [22]), but featuring different heating methods. A scan with $f_0(\%)$ is performed with $a = 1.2$ (limiter configuration), $\tau_E^{-1/9} \approx 1$, $g_* = 4$ (Carbon), and respectively $P(MW) = 2.5, 11.5, 12$, $Z_{eff} = 1.5, 1.6, 1.4$ for the ohmic, ICRH, NBI cases. The model well predicts the increase of the ohmic DL obtained with the addition of ICRH and NBI, equivalently. On the contrary, the n_G criterion cannot explain such a large difference of the DL in shots that share the same I_p. We also mention figure 161 of [23], referring to this kind of

experiments, where a clear trend $P^{0.5}$ is observed for the edge DL: this confirms that the phenomenon occurs at the edge, as predicted by (15)-(18). In conclusion, our model describes quite well the JET L-mode DL.

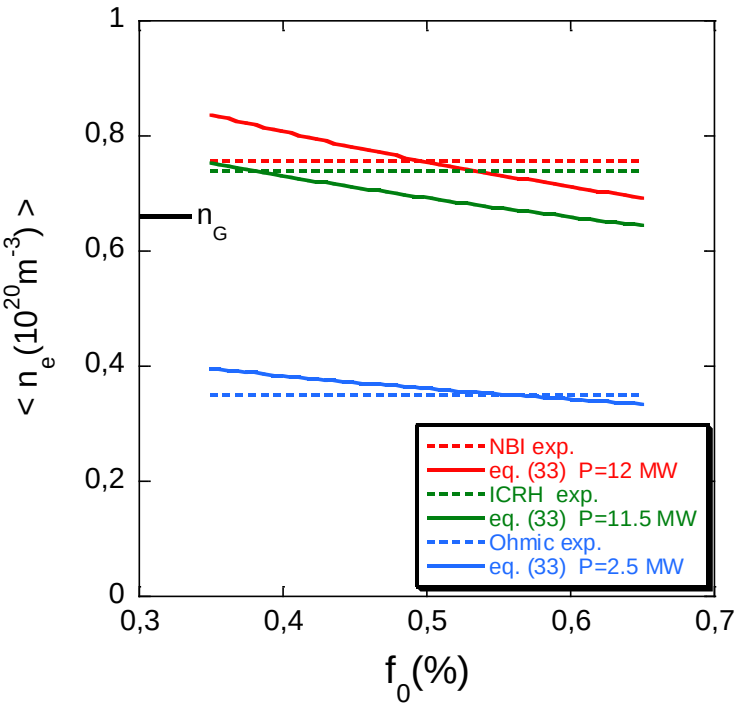

Figure 3. Scan with $f_0(\%)$ of model (33) (continuous lines; parameter setting in the text), alongside experimental $\langle n_e \rangle_{DL}$ (dashed lines). The value $n_G \cong 0.66$ of these experiments is also reported.

4.4 Further L-mode tokamak experiments

An inter-machines analysis, collecting together published DL data from several L-mode, NBI experiments is shown in figure 4. The data scattering is substantially reduced when replacing, as order parameter, n_G by model (33) (we take $C = 0.45$), even further reducing it to just the P, I_p dependences, the only choice, since Z_{eff} is not given on a shot-by-shot basis. Compared to the similar analysis reported in [2], here we add a further TEXTOR experiment, and we include the $\tau_E^{-1/9}$ factor within model (33), by taking representative values of τ_E for each device as given by the standard thermal L-mode scaling law [4]. A power-law fit of these data also confirms the model (33):

34) $(\bar{n}_e)_{DL}(10^{20} m^{-3}) \approx 0.58 \times [P(MW)/(\pi\, a^2)]^{0.49\pm0.02}\, {n_G}^{0.44\pm0.04}\, B_\phi^{-0.12\pm0.04}$,

The three variables in (34) have a weak linear Pearson correlation ($|r| = 0.2, 0.26, 043$ respectively for the first two, the first and the third, the last two). The dependence on the toroidal field is found almost negligible, as in the model.

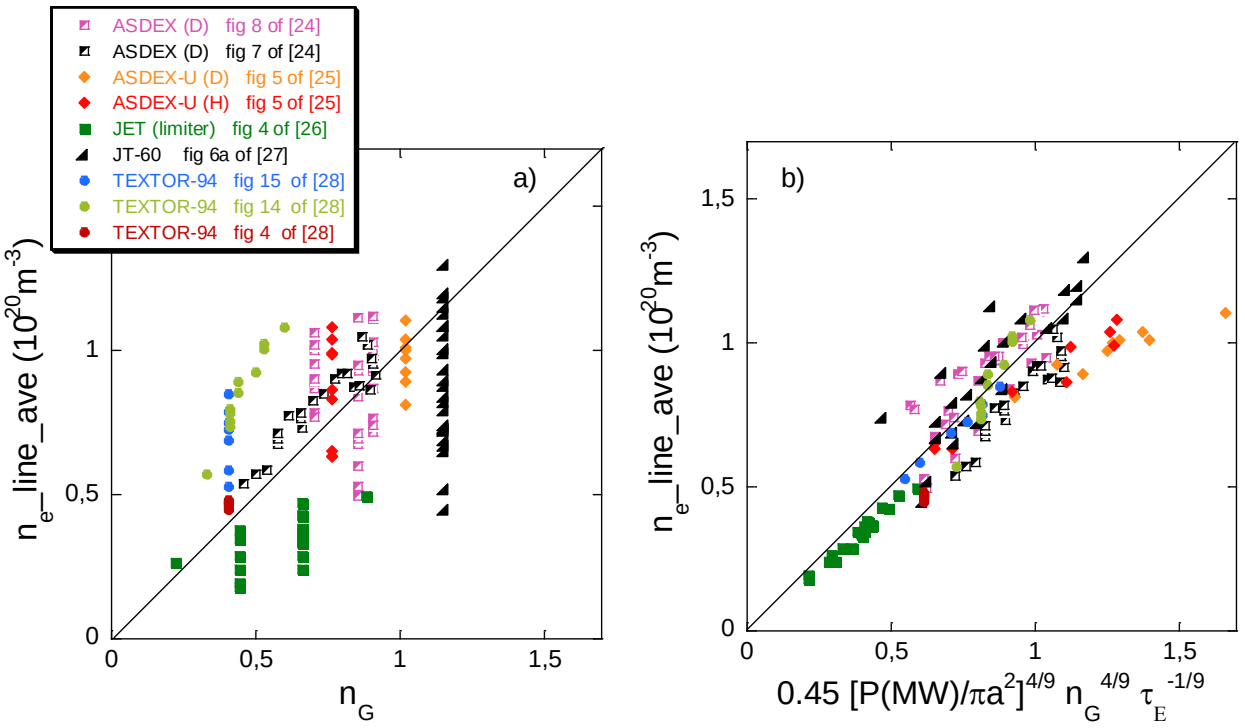

Figure 4. Maximum published line-average densities obtained in several L-mode NBI experiments. The legend reports the data source. They are plotted vs. n_G in (a), and vs (33) w/o the Z_{eff} term in (b).

To our knowledge, the only published result against the P dependence of the tokamak L-mode DL, or at least of the 'detachment DL', is figure 9a of [29], referring to DIII-D experiments ($a = 0.63$, $R_0 = 1.66$) and showing the densities at the plasma detachment $(\bar{n}_e)_{det}$, in both ohmic and NBI discharges. A criticism has been raised in [2] to that figure: here, we present again our counter analysis, with some new elements. An unbiased look at the plotted data suggests an inverse dependence on B_ϕ. In fact, we get $(\bar{n}_e)_{det}(10^{20}m^{-3}) \approx 0.64 \times [P(MW)/(\pi\, a^2)]^{0.31\pm0.07}\, {n_G}^{0.74\pm0.09}\, B_\phi^{-0.45\pm0.09}$ for the NBI subset, and $(\bar{n}_e)_{det}(10^{20}m^{-3}) \approx 0.84 \times {n_G}^{1.45\pm0.11}\, B_\phi^{-0.37\pm0.14}$ for the ohmic subset. In the latter, P is not considered as fitting variable, being strongly linearly correlated with I_p. Note that the B_ϕ exponent is the same in the two subsets, supporting a real physical dependence. Detachment is not necessarily close to the DL in these experiments: it is qualitatively reported that $(\bar{n}_e)_{det} \cong (\bar{n}_e)_{DL}$ at low/moderate edge safety factor

q_{95}, whereas $(\bar{n}_e)_{det} < (\bar{n}_e)_{DL}$ at high q_{95}. Since q_{95} plays a role, in the previous two fits we replace B_ϕ by the cylindrical approximation of the edge safety factor: $B_\phi = \pi\, R_0\, n_G\, q_a/5$. For the NBI and the ohmic subsets we get respectively

35) $$(\bar{n}_e)_{det}(10^{20}m^{-3}) \approx 0.43 \times [P(MW)/(\pi\, a^2)]^{0.31\pm0.07}\, {n_G}^{0.29\pm0.17}\, (q_a/\overline{q_a})^{-0.45\pm0.09}$$

36) $$(\bar{n}_e)_{det}(10^{20}m^{-3}) \approx 0.66 \times\, {n_G}^{1.1\pm0.15}\, (q_a/\overline{q_a})^{-0.37\pm0.14}$$

with $\overline{q_a}$ the shot-average value in each of the two subsets. Apart from the q_a dependence, possibly related to the fact of considering $(\bar{n}_e)_{det}$ instead of $(\bar{n}_e)_{DL}$, and the unknown Z_{eff} dependence, (35) is similar to the model (33), and (36) to the ohmic version ($P{\sim}I_p$) of the same. In any case, the NBI scaling (35) is much closer to the previous fit (34) than to the n_G criterion. We draw the conclusion that these data indeed support the P dependence of the tokamak L-mode DL. The comparison between (34), (35) also suggests that the 'ultimate DL' has a simpler form than the 'detachment DL', in consonance with the general premise stated in the introduction.

4.5 Wendelstein 7-X

Scaling laws similar to (23) and based on the present model have been successfully compared to LHD data in [1] and to Wendelstein 7-X in [30, 31]. Here, we consider the maximum values for the Wendelstein 7-X edge density ($r_*/a = 0.85$) reported in figure 4 of [31], and, in particular, those obtained after boronization ($Z_{eff} < 2$), which show the highest DL. They refer to the standard configuration: $R_0 = 5.5$, $a = 0.51$, $B_\phi = 2.41$, $\iota_{2/3} = 0.9$. Figure 5 shows that the modelled edge DL, $n_* = n_1 \times \Theta(2\delta_n^2 n_1^2/n_2^2)$, with both scaling laws (26) (black line) and (23) (red line) for n_1, agrees fairly well with those densities. The quantities n_1, n_2 are computed as follows. For the two most important parameters we take values representative of clean machine condition: $Z_{eff} = 1.5$, $f_0(\%) = 0.5$. A mixture of Boron-Carbon-Oxygen in equal concentrations is considered, giving $g_{I*} = 3.74$; $\mathcal{F}_{bulk}$ is computed for $T_* = 0.2keV$ and $T_0 = 2keV$ [7]. The estimate $\Psi_p^{-0.4} \approx 3.62 \times \delta_T^{0.544}\, \delta_n^{-0.396}\, \delta_{Rad}^{0.375}$ given in [2] is applied in (23), with $\delta_T = 0.4$ (half way between a parabolic and a quartic profile), δ_n derived from the experimental data of the same figure 4 of [31], and $\delta_{Rad} =$

$\int_0^a dr\, r\, \Re / \int_{r*}^a dr\, r\, \Re \cong 1 + [T_* a/2(a - r_*)]\delta_n^2\, \mathcal{F}_{bulk}/G_*$ (it is estimated δ_{Rad}~1.2). The shape factor in (26) is estimated by $\Im_p{}^{-1/2} = \Psi_p{}^{-1/2}\delta_{nT}{}^{1/2} \sim \Psi_p{}^{-1/2}\delta_T{}^{1/2}\delta_n{}^{1/2}$. Finally we set $\lambda_{tok} = \left(\hat{V}_\phi\, q_0\right)_{tok} = 0.41$, as average estimate on the previous JET database.

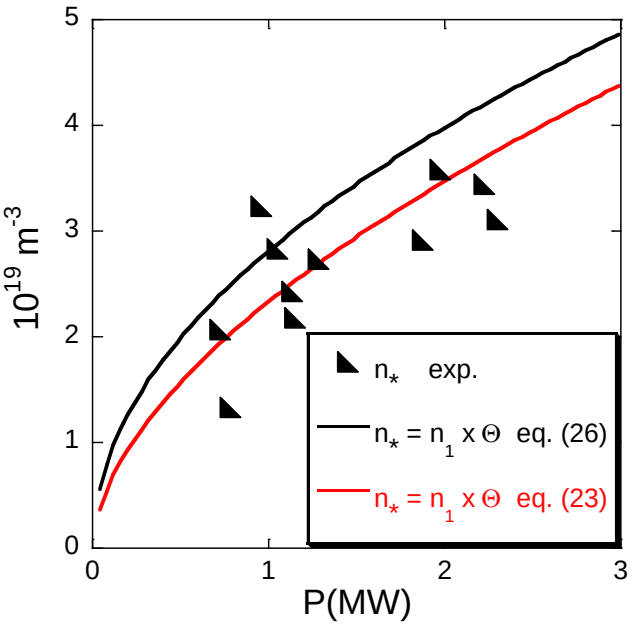

Figure 5. Symbols: experimental edge DL from figure 4 of [31]. Lines: predicted edge DL, $n_* = n_1 \times \Theta$, with n_1 given by (26) (black) and (23) (red). Details of parameters setting in the text.

5. Conclusions

A basic power balance model, exploiting just two equations, i) 1D single-fluids heat transport, ii) on-axis ohm's law with Spitzer resistivity (in a suitable limit for the stellarator), gives a satisfactory description of the maximum observed densities in the main configurations. The generality stems from the minimal 1D physics involved and from taking integrals of i), hence smoothing out the profile peculiarities of the different configurations. The model predicts a Sudo-like scaling law for the Stellarator and the same Greenwald-like scaling law for the tokamak and the RFP. Unlike the respective empirical relations, they feature also dependences on Z_{eff}, shape factors, and (normalized) heating power in the tokamak case. These scaling laws are obtained without any hypothesis for the transport. As far as the tokamak and the RFP are concerned, we get a tenuous dependence on the energy confinement time τ_E, giving almost the same quantitative prediction in the two configurations. Moreover, our analysis contradicts the widespread vision of a DL representable by the *single* parameter n_G, since the estimates obtained by the proposed model are clearly better. In particular, we have devoted ample space to bring evidences in favour of the *P* dependence in the L mode tokamak, including JET limiter experiments, not discussed in the previous paper [2], which demonstrate, *at*

comparable Z_{eff}, a substantial increase of the ohmic DL obtained by NBI and ICRH in a complete equivalent way [22]. Finally, we also showed, as done in [2], that careful analyses of published data, supposed to be a validation of the n_G criterion, confirm, instead, the present model.

Acknowledgement

We thank M. E. Puiatti for helpful discussions.

References

[1] P. Zanca et al, Nucl. Fusion **57** (2017) 056010

[2] P. Zanca et al, Nucl. Fusion **59** (2019) 126011

[3] F. W. Perkins, R. A. Hulse, Physics of Fluids **28** (1985) 1837

[4] J. A. Wesson, Tokamaks, 3rd edition (2004) (Oxford: Clarendon)

[5] D. Ashby, M. Hughes, Nucl. Fus. 21 (1981) 911

[6] S. Sudo et al, Nucl. Fusion **30** (1990) 11

[7] T. Klinger et al, Nucl. Fusion **59** (2019) 112004

[8] S. Cappello, D. Bonfiglio, D. F. Escande, Phys. Plasmas **13** (2006) 056102

[9] M. Greenwald, Plasma Phys. Contr. Fusion **44** (2002) R27

[10] U. Stroth, et al, Nucl. Fusion **36** (1996) 1063

[11] J. Miyazawa et al, Nucl. Fusion **48** (2008) 015003

[12] Chung H.-K., Chen M.H., Morgan W.L., Ralchenko Y. and Lee R.W. 2005 *High Energy Density Phys.* **1** 3–12

[13] Atomic Molecular Data Services, https://www-amdis.iaea.org/FLYCHK/

[14] M. E. Puiatti *et al*, Phys. Plasmas **16** (2009) 012505

[15] G. Spizzo *et al*, Nucl. Fusion **55** (2015) 043007

[16] F. Auriemma *et al*, *Nucl. Fusion* **55** (2015) 043010

[17] L. Carraro *et al*, 32nd EPS Conference on Plasma Phys. Tarragona (2005) ECA Vol. 29C, P-2.003

[18] M. Valisa *et al*, Fusion Energy 2004, Proc. 20th Int. Conf. Villamoura, 1-6 November 2004 (Vienna: IAEA) [EX/P4-13], http://www-naweb.iaea.org/napc/physics/fec/fec2004/datasets/index.html

[19] G. Pucella et al, Nucl. Fusion **53** (2013) 083002

[20] M. Groth et al, Nucl. Fusion **53** (2013) 093016

[21] A.Huber et al, J. Nucl. Mater. **438** (2013) S139

[22] J. Jacquinot et al, Fusion Engineering and Design **12** (1990) 245-250

[23] Jet Joint Undertaking Progress Report, 1989

[24] A. Stabler et al, Nucl. Fusion 32 (1992) 1557

[25] V. Mertens et al, Nucl. Fusion 37 (1997) 1607

[26] G. Duesing and the JET Team, Plasma Phys. Contr. Fusion 28 (1986) 1429

[27] Y. Kamada et al, Nucl. Fusion 31 (1991) 1827

[28] J. Rapp et al, Nucl. Fusion 39 (1999) 765

[29] T. W. Petrie *et al*, *Nucl. Fusion* **33** (1993) 929

[30] G. Fuchert *et al*, "Density related operational limit in the limiter phase of Wendelstein 7-X", 2017 European Conference on Circuit Theory and Design (ECCTD, Catania, Italy), IEEE (2017)

[31] G. Fuchert *et al*, Nucl. Fusion **60** (2020) 036020